Int. J. Heat Mass Transfer. Vol. 36, No. 6, pp. 1517–1528, 1993
Printed in Great Britain

0017-9310/93 $6.00 + 0.00

Three-dimensional natural convection in an enclosed vertical rod bundle with mixed boundary conditions

Y. F. RAO and E. K. GLAKPE
Department of Mechanical Engineering, Howard University, Washington, D.C. 20059, U.S.A.

(*Received* 12 *August* 1991 *and in final form* 13 *July* 1992)

Abstract—Numerical solutions in boundary-fitted coordinates are presented for the problem of three-dimensional natural convection in an enclosed vertical rod bundle. The rod bundle is composed of seven hot rods placed in an isothermal cold hexagonal enclosure with the rod surfaces heated under uniform heat flux conditions. Flow fields and temperature distributions are obtained for Rayleigh numbers up to 10^8 and a Prandtl number of 0.7; the aspect ratio of vertical to horizontal dimensions is set at the value of unity. The distributions of velocities and isotherms are presented. The effect of natural convection on local and average boundary temperatures as well as on heat transfer coefficients is examined. With an increase in the Rayleigh number, the rods tend to achieve nearly the same average boundary temperature, or consequently the same overall heat transfer coefficient. It is demonstrated that in the boundary-layer regime, the Nusselt and Rayleigh numbers can well be correlated with $Nu = cRa^{1/4}$, which coincides with that for a vertical rectangular channel. The results are compared with those for an isothermal rod bundle to examine the effect of boundary conditions on the flow distribution and heat transfer.

INTRODUCTION

THREE-DIMENSIONAL, buoyancy-induced natural convection in enclosures, or so-called three-dimensional buoyant enclosure flow [1], has been receiving considerable attention due to its potential applications as well as practical importance in engineering designs and energy related problems. However, most of the published studies, e.g. [2–4], only deal with basic geometries such as rectangular boxes and cylindrical annuli, to which conventional coordinate systems such as the cartesian or polar coordinates can be adopted to discretize the governing equations into finite-difference ones without much difficulty. The abundance of reports on these basic geometries is partly due to fundamental importance of the rectangular or cylindrical enclosure problems and, on the other hand, partly because of the geometric complexity involved in geometries like the present one.

Natural convection in an enclosed space composed of a hot vertical rod bundle placed in a cold enclosure has potential applications including the storage of heat-generating spent-fuel assemblies, and heat removal of a nuclear fuel-pin configuration in a light-water reactor in situations of emergency. Keyhani *et al.* [5] studied experimentally the free convection heat transfer in a rod bundle. Chen *et al.* [6] developed a numerical scheme for forced convective heat transfer in the same geometry as the present one. To the authors' knowledge, no numerical studies have been published for three-dimensional natural convection in an enclosed rod bundle despite its importance in engineering problems such as the ones mentioned above. This study is the first that simulates three-dimensional buoyant enclosure flow in a closed, multi-connected space such as the vertical bundle considered in the present study.

In order to simulate natural convection conditions, modifications are made to the computational scheme of Chen *et al.* [6] developed to study longitudinal or axial forced convective flow in a rod bundle. Instead of the Chorin scheme [7] adopted by Chen *et al.* in their numerical scheme for parabolic problems [6] and shown to be unsuitable for solving elliptic natural convection problems [8], the SIMPLE algorithm [9] is employed for the pressure-correction part of the scheme in solving the resulting finite difference approximations to the transformed elliptic governing equations. The numerical solutions are obtained in boundary-fitted coordinates similar to that adopted in ref. [6].

The purpose of the present paper is to study the effects of three-dimensional buoyant enclosure flow in an enclosed rod bundle when a uniform heat flux is applied to the rod surfaces while the enclosure wall is maintained at a constant temperature and the top and bottom ends are insulated. Results are presented for Rayleigh numbers up to 10^8 and a Prandtl number of 0.7. Flow fields, isotherm patterns, local and average boundary temperatures as well as heat transfer coefficients obtained exhibit distinct differences from the results for a rod bundle with the rod surfaces and the enclosure wall being isothermal but at different temperatures [10]. This indicates significant influences

NOMENCLATURE

a a positive coefficient prescribing the linear transformation in the axial (z) direction, $dz/d\zeta = 1/a$
c_p specific heat at constant pressure
d' distance between two adjacent rods
d aspect ratio, d'/L'
g gravitational acceleration
Gr Grashof number, $g\beta_f L'^4 q'_0/(\nu^2 k)$
h dimensionless specific enthalpy, h'/h'_0
H' enclosure height
H aspect ratio, H'/L'
k thermal conductivity
L' half enclosure (flat-to-flat) width
Nu Nusselt number, $q'_0 L'/(T'-T'_c)k'$
p dimensionless pressure, $(p'-p'_s)/\rho_0 V'^2_0$
Pr Prandtl number, ν/α_f
q' heat flux
q'_0 constant heat flux across the rod surfaces
q dimensionless heat flux, $q'Pr/\rho'_0 h'_0 V'_0$
Ra Rayleigh number, $Gr\,Pr$
t' time
t dimensionless time, $t'V'_0/L'$
T' temperature
T dimensionless temperature, $(T'-T'_0)k/(q'_0 L')$
u, v, w dimensionless velocities scaled by V'_0
V'_0 reference velocity, ν/L'
V_{2D} velocity projection on a vertical or horizontal plane
$V_{2D,max}$ maximum value of V_{2D}
x, y, z dimensionless Cartesian coordinates scaled by L'.

Greek symbols
α_f thermal diffusivity
β_f volumetric expansion coefficient
α, β, γ coordinate transformation coefficients
ν kinematic viscosity
ξ, η, ζ coordinates in the transformed geometry
ρ density
Σ shear stress tensor.

Superscripts
$'$ dimensional quantity
$\sim$ variable in the transformed coordinates
$-$ averged quantity.

Subscripts
c cold enclosure
h hot rod
0 reference state
R1 Boundary of Rod 1 or the central rod
R2 Boundary of Rod 2 or the outer rod
s static value
1, 2, 3 reference to ξ, η and ζ coordinates
ξ, η, ζ, t first partial derivatives.

of boundary conditions on heat transfer and fluid flow in this geometry.

GOVERNING EQUATIONS AND NUMERICAL PROCEDURE

The geometry of the problem is schematically shown in Fig. 1, where seven hot vertical rods are enclosed in a cold vertical hexagonal enclosure filled with fluid. The hot rod surfaces are subject to a uniform heat flux q'_0 while the cold enclosure wall is maintained at a constant temperature T'_c. The top and bottom boundaries of the enclosure are assumed adiabatic. The ratio of the height H' to the half-width L' of the enclosure ($H = H'/L'$) is chosen as unity. The ratio of rod radius R' to L' ($R = R'/L'$) is taken as 3/11, and that of the gap d' between two rods to L' ($d = d'/L'$) 1.9/11, according to the data in ref. 6 which is based on an experimental assembly. Due to the symmetrical nature of the problem, only one twelfth of the assembly, i.e. the domain between symmetry planes O-A and O-B, is utilized for the solution of the three-dimensional, steady-state natural convection problem.

For the present geometry, a numerically generated, boundary-fitted coordinate system is adopted based on the curvilinear coordinate transformation algorithm of Thompson [11]. The coordinate system allows the relevant boundary conditions to be represented accurately without resorting to otherwise unavoidable interpolations. It is generated by solving a system of elliptic partial differential equations given as follows:

$$\alpha x_{\xi\xi} - 2\beta x_{\xi\eta} + \gamma x_{\eta\eta} = -J_{12}^2[x_\xi P(\xi,\eta) + x_\eta Q(\xi,\eta)] \quad (1)$$

$$\alpha y_{\xi\xi} - 2\beta y_{\xi\eta} + \gamma y_{\eta\eta} = -J_{12}^2[y_\xi P(\xi,\eta) + y_\eta Q(\xi,\eta)] \quad (2)$$

where the transformation coefficients and Jacobian are

$$\alpha = x_\eta^2 + y_\eta^2, \quad \gamma = x_\xi^2 + y_\xi^2,$$

$$\beta = x_\xi x_\eta + y_\xi y_\eta, \quad J_{12} = x_\xi y_\eta - x_\eta y_\xi. \quad (3)$$

The functions P and Q in equations (1) and (2) are coordinate control functions that may be used to cause the coordinate lines to concentrate in certain parts of the computational domain. With the existing numerical code [6], a grid system composed of (x, y)

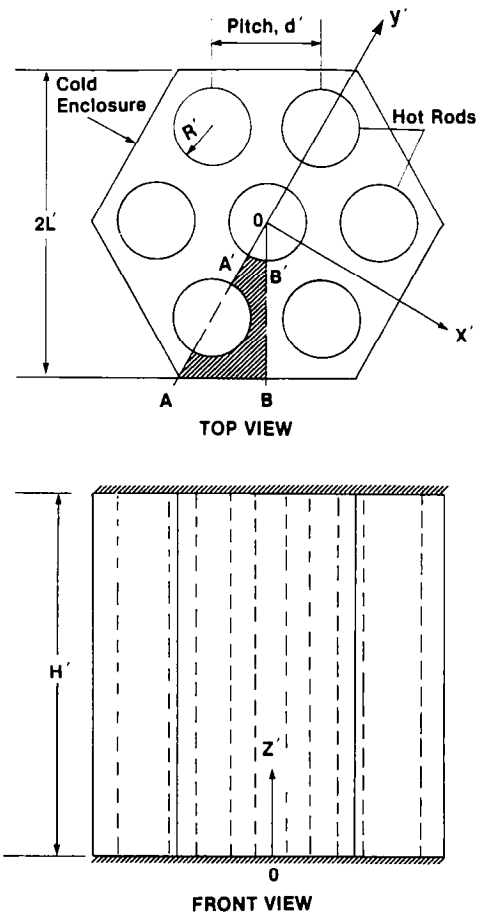

FIG. 1. Flow geometry and computational domain.

values corresponding to discrete values of ξ and η is generated, with all boundary lines, solid or symmetrical, being specified on either constant-ξ and/or constant-η lines, as shown in Fig. 2. The third (axial) coordinate is simply transformed as $dz/d\zeta = 1/a$ where a can be a constant or variable depending on whether or not the grid spacing in physical coordinate z is chosen to be uniform.

Table 1. Expressions for coefficients in the generic transformed equation, equation (4)

ϕ	b^ϕ	c^ϕ	e^ϕ	S^ϕ
1	0	0	0	0
u	$-y_\eta p+\tilde{\Sigma}_{11}$	$y_\xi p+\tilde{\Sigma}_{12}$	$\tilde{\Sigma}_{13}$	0
v	$x_\eta p+\tilde{\Sigma}_{21}$	$-x_\xi p+\tilde{\Sigma}_{22}$	$\tilde{\Sigma}_{23}$	0
w	$\tilde{\Sigma}_{31}$	$\tilde{\Sigma}_{32}$	$-p+\tilde{\Sigma}_{33}$	$-Gr\,T$
h	$-\tilde{q}_1/Pr$	$-\tilde{q}_2/Pr$	$-\tilde{q}_3/Pr$	0

The transformed, dimensionless governing equations, i.e. the continuity, x-, y- and z-momentum, and energy equations, are written in the following generic form:

$$\int_V (\rho\phi)_t \frac{J_{12}}{a}\,dV + \int_{S_\xi} \rho\tilde{u}\phi\,\frac{1}{a}\,d\eta\,d\zeta + \int_{S_\eta} \rho\tilde{v}\phi\,\frac{1}{a}\,d\xi\,d\zeta + \int_{S_\zeta} \rho\tilde{w}\phi J_{12}\,d\xi\,d\eta = \int_{S_\xi} b^\phi\,\frac{1}{a}\,d\eta\,d\zeta + \int_{S_\eta} c^\phi\,\frac{1}{a}\,d\xi\,d\zeta + \int_{S_\zeta} e^\phi J_{12}\,d\xi\,d\eta + \int_V S^\phi\,\frac{J_{12}}{a}\,dV \quad (4)$$

in which ϕ represents the transport variable; the coefficients and source terms b^ϕ, c^ϕ, e^ϕ and S^ϕ are given in Table 1.

In the generic equation, S_ξ, S_η and S_ζ represent the two control volume surfaces of constant ξ, η and ζ respectively; dV is the volume element bounded by these surfaces. A Grashof number based on the half width of the enclosure (L') is defined as $Gr = g\beta_f L'^4 q'_0/(\nu^2 k)$. Other symbols have their usual physical meanings. The equation of state is that of a perfect

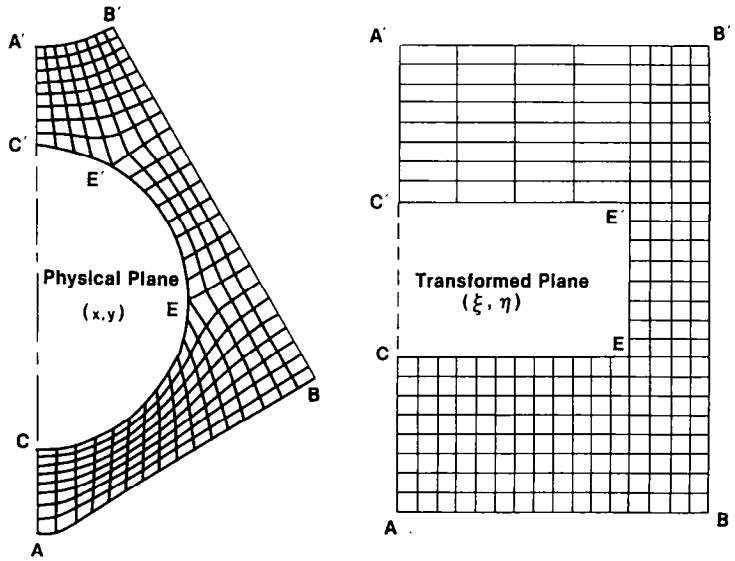

FIG. 2. Grid systems in the physical and transformed planes.

gas which in dimensionless terms is $T = h$. The Prandtl number is fixed at 0.7. The variables with the '~' symbol represent variables in the transformed region. Their relationships with the variables in the physical region (those without the '~' symbol) are given in the following matrix equation with heat flux q as an example:

$$\begin{bmatrix} \tilde{q}_1 \\ \tilde{q}_2 \\ \tilde{q}_3 \end{bmatrix} = \begin{bmatrix} y_\eta & -x_\eta & 0 \\ -y_\xi & x_\xi & 0 \\ 0 & 0 & 1 \end{bmatrix} \begin{bmatrix} q_1 \\ q_2 \\ q_3 \end{bmatrix}. \quad (5)$$

In the matrix equation, subscripts 1, 2, 3 represent either x-, y-, z- or ξ-, η-, ζ-directions. Substituting $[q_1, q_2, q_3]$ in equation 5 with $[u, v, w]$ we have relationships for velocities, or with $[\Sigma_{i1}, \Sigma_{i2}, \Sigma_{i3}]$ for the terms of the viscous stress tensor ($i = 1$ for x-, $i = 2$ for y- and $i = 3$ for z-momentum equations). The heat flux q is related to temperature T through Fourier's law as

$$\begin{bmatrix} \tilde{q}_1 \\ \tilde{q}_2 \\ \tilde{q}_3 \end{bmatrix} = -\frac{k}{J_{12}} \begin{bmatrix} \alpha & -\beta & 0 \\ -\beta & \gamma & 0 \\ 0 & 0 & aJ_{12} \end{bmatrix} \begin{bmatrix} T_\xi \\ T_\eta \\ T_\zeta \end{bmatrix}. \quad (6)$$

Except for the buoyancy terms expressed with the Boussinesq approximation in the momentum equations, the governing equations are similar to those presented in ref. [6], in which other details can be found.

The rod boundaries and enclosure walls including the top and bottom ends are modelled as no-slip surfaces with vanishing velocities. A constant heat flux q_0 is assigned to all rod surfaces while zero heat flux ($q = 0$) is assumed at the top and bottom boundaries. The uniform temperature on the cold enclosure wall has the value of 0 from the definition of the dimensionless temperature. For the symmetrical boundaries O-A and O-B (Fig. 1), the concept of mirror image reflection [12] is utilized that extends the computational domain one grid beyond the symmetry lines. The application of the concept to the present case results in the following relationships [10]:

$$(V_{2D})_W = (V_{2D})_E; \quad \theta_W + \theta_E = (2n+1)\pi + 2\phi. \quad (7)$$

In the above equation, $V_{2D}[= (u^2+v^2)^{1/2}]$ is the projection of the velocity vector on a horizontal (x–y) plane; θ is the angle of V_{2D} with the positive x-axis; n is any integer; and ϕ is the angle of a symmetry line measured from the negative y-axis, thus $\phi = 0$ for the line O-A in Fig. 1 and $\phi = \pi/6$ for the line O-B. The subscripts E and W denote grid points that are mirror images of each other to the EAST and WEST respectively of the symmetry line. Equation (7) gives the symmetry condition for u and v. The symmetry condition for the other variables (f's) is simply, $f_W = f_E$.

The equations for the finite difference approximations to the integral equations, equation (4), are derived with a grid system that in three dimensions staggers the grid point for temperature, pressure and density a half-grid spacing away from the grid point for the velocity components. One of the advantages of the grid system is that no boundary condition is needed for pressure. The SIMPLE algorithm [9] is utilized for the pressure and velocity corrections that link the continuity equation directly with the momentum equations. The resulting pressure-correction equation is similar to that derived for solving the problem of natural convection about a vertical square rod placed in a cylindrical enclosure [13]. Solutions of the finite-difference equations are carried out iteratively with the SOR scheme. The iteration is continued until for each grid point or control volume, the relative changes per iteration step for variables including the velocity components, temperature and pressure are less than 10^{-5} and the mass residual is less than 10^{-4}. Relaxation factors are chosen between 0.4 and 1.5 depending on the Rayleigh number. For all Rayleigh numbers, a grid distribution of $19 \times 25 \times 15$ is adopted based on the analysis of accuracy and the grid-spacing-effect for a similar scheme [8]. In order to better satisfy the top and bottom boundary conditions, a non-uniform grid distribution along the z- or ζ-direction, formulated as $\Delta z_{i+1} = c\Delta z_i$ (c = constant), is chosen such that the grid points are doubly concentrated near the top and bottom boundaries than around the mid-height; this makes the grid spacing near the boundaries equivalent to that of a system of 21 uniform grid points along the vertical direction. The code is also verified by examining the total energy balance, i.e. the difference between the total heat fluxes from the hot rods and that across the cold enclosure. This difference generally increases as the Rayleigh number is increased, with the maximum being 2.8% in the range of Rayleigh numbers considered in the present study. A typical run on an IBM 3090 serial system required about 90 CPU minutes.

RESULTS AND DISCUSSION

Flow fields and temperature distributions

Numerical results have been obtained for Rayleigh numbers ranging from 10^2 to 10^8. This range includes different convection intensities of pseudo-conduction, transitional convection and boundary-layer regions.

Figure 3 shows isotherms for $Ra = 10^2$ on three horizontal planes at axial levels $z = 0.1H$, $z = 0.5H$ and $z = 0.9H$ respectively. Temperature is normalized such that it has the value of unity where the maximum temperature in the three-dimensional domain occurs, and the value of zero at the cold enclosure wall which is represented by line A-B in a horizontal plane. Nine isotherms are shown ranging from 0.1 to 0.9 with the increment being 0.1. It should be noted that unlike the case of isothermal boundary conditions, isotherms obtained do not coincide with the rod boundaries; they start or end on these surfaces. At this low Rayleigh number, the effect of convection is clearly insignificant and the temperature distributions in the three planes are indistinguishably similar to each other and almost identical to that of pure conduction. This state

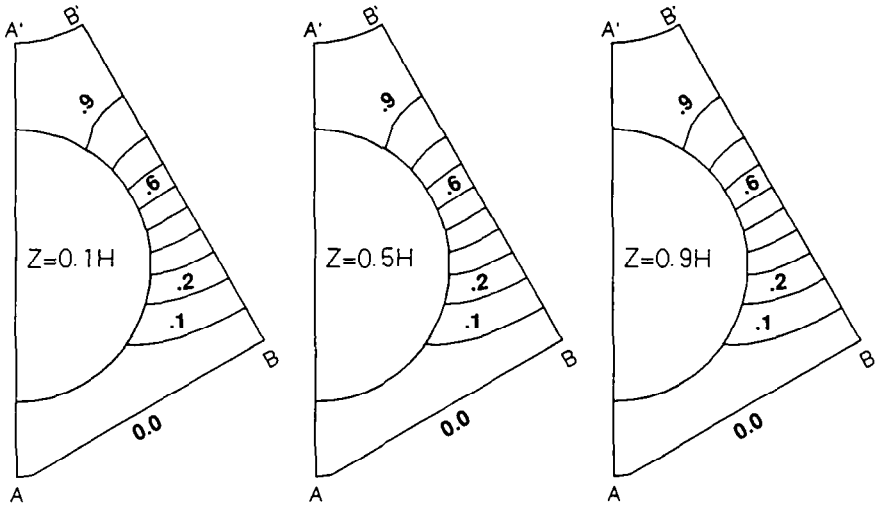

FIG. 3. Isotherms at selected lower, middle and upper horizontal planes for $Ra = 10^2$.

is referred to as pseudo-conduction. Two major differences from the case of isothermal boundary conditions can be observed; first, there is no thermally-stagnant 'hot region' existing between the central and outer rods where heat transfer is minimum; second, there is a 'cold region' between the outer rod and the enclosure wall where temperatures are between 0.0 and 0.1. These are natural consequences of the uniform-heat-flux boundary condition on the rod surfaces. This pseudo-conduction state remains until the Rayleigh number is increased above about 10^3 and, as will be discussed later, disappears when natural convection is developed at higher Rayleigh numbers.

Shown in Figs. 4–6 are velocity fields and isotherms for $Ra = 10^5$ at three axial levels and two symmetry planes, A'-A and B'-B respectively. The cold surface is represented by the right vertical side in vertical planes. The results shown in Figs. 4–6 present the case in which natural convection is fairly developed but boundary layer flow is not yet realized. In plane B'-B as shown in Fig. 4, the velocity field looks similar to that in the case of isothermal boundary conditions; it is a circulating flow driven by an ascending flow near the central hot-rod boundary (on the left side) and a descending flow near the cold enclosure wall (on the right side), with the cold fluid down from the cold wall flowing toward the central hot-rod boundary in the bottom-end region, and vice versa in the top-end region. The isotherm pattern obtained in this study, however, is different from the case of isothermal

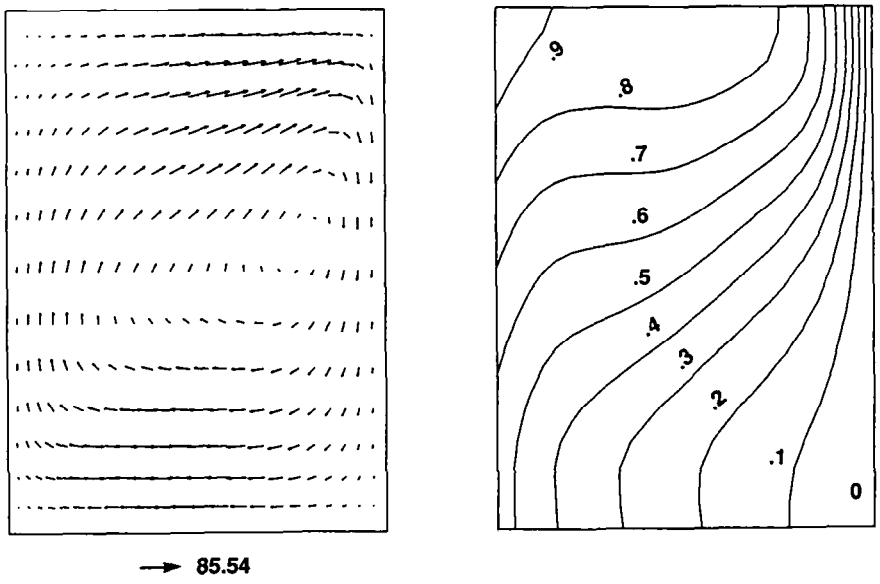

FIG. 4. Velocities and isotherms at the vertical symmetry plane B'-B for $Ra = 10^5$: $V_{2D,max} = 85.54$.

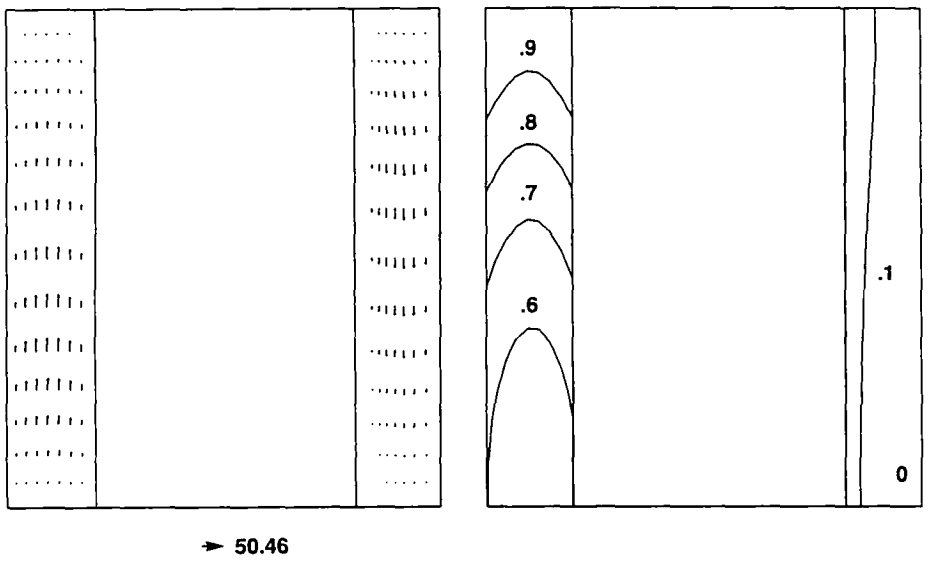

FIG. 5. Velocities and isotherms at the vertical symmetry plane A′-A for $Ra = 10^5$: $V_{2D,max} = 50.46$.

boundary conditions in that some of the isotherms start or end on the hot rod surfaces; and due to the constant-heat-flux condition, the isotherms tend to distribute uniformly along the rod surfaces. The differences are more significant in the velocity field and temperature distributions in plane A′-A as shown in Fig. 5; no upward flow can be found between the outer hot rod and the cold wall. The flow there is uniformly downward since for this moderate Rayleigh number the fluid region between the two surfaces is still cold—only one isotherm of value 0.1 appears in this region. The flow between the two hot rods, on the other hand, is uniformly upward. Four isotherms, of values 0.6–0.9 from bottom to top, appear in this region, which suggests the cooling down of this area compared to the pseudo-conduction state in which temperatures at all grid points in this area are above 0.9 (Fig. 3). Figure 6(a) shows velocity fields at three axial levels. At the lower horizontal plane ($z = 0.1H$), the cold fluid down from the cold wall A-B flows toward the 'hot region' between the central and the outer hot rods to be heated and then to flow upward. The corresponding isotherm plot in Fig. 6(b) shows that this flow cools down the hot region. At the upper horizontal plane ($z = 0.9H$), on the other hand, the fluid from the hot region flows toward the cold wall to be cooled and then to flow downward in the axial or vertical direction in completing the main circulation. Due to the heating effect of the hot fluid, the hot region spreads toward the cold enclosure wall; the 'cold region' that exists between the outer rod and the cold wall for low Rayleigh numbers (Fig. 3) disappears. At the middle plane ($z = 0.5H$), since the flow is mainly along the axial or vertical direction, the velocities in the horizontal plane are very small. It is interesting to notice that in this plane, velocities near the 'hot region' and those near the cold wall are toward each other because of the 'heating' effect of the outer hot rod. This flow structure is similar to that obtained under isothermal heating conditions. The isotherm plots however present differences between the two cases. In the case of isothermal boundary conditions, since temperatures at the rod boundaries are fixed at the value of 1.0, nine isotherms ranging 0.1–0.9 always appear in every horizontal plane, although the development of natural convection affects their distributions. In the case of mixed boundary conditions, on the other hand, fewer isotherms appear in the lower plane than in the upper plane as a result of developed natural convection. In the plane $z = 0.1H$, for example, only five isotherms of values 0.1–0.5 appear compared to nine (0.1–0.9) in the plane $z = 0.9H$. This indicates that thermal stratification with temperatures varying from low to high along the vertical direction is more likely to be developed in the case of mixed boundary conditions than in the case of isothermal boundary conditions.

Figures 7–9 show velocity fields and isotherms for $Ra = 10^7$. This is the case in which natural convection is developed to such extent that boundary layer flows become dominant. This is evidently shown in Fig. 7 by the distributions of velocities and isotherms near the cold wall and the hot rod surface. The outer hot rod, i.e. the rod between the central rod and the enclosure wall, affects this circulating flow (Fig. 7) such that weak secondary flows appear in the core region which otherwise would have been more or less stagnant. These secondary flows are basically the same as those observed in the case of isothermal boundary conditions; their vertical positions shift downward as the Rayleigh number is further increased. An obvious thermal stratification develops from the top boundary

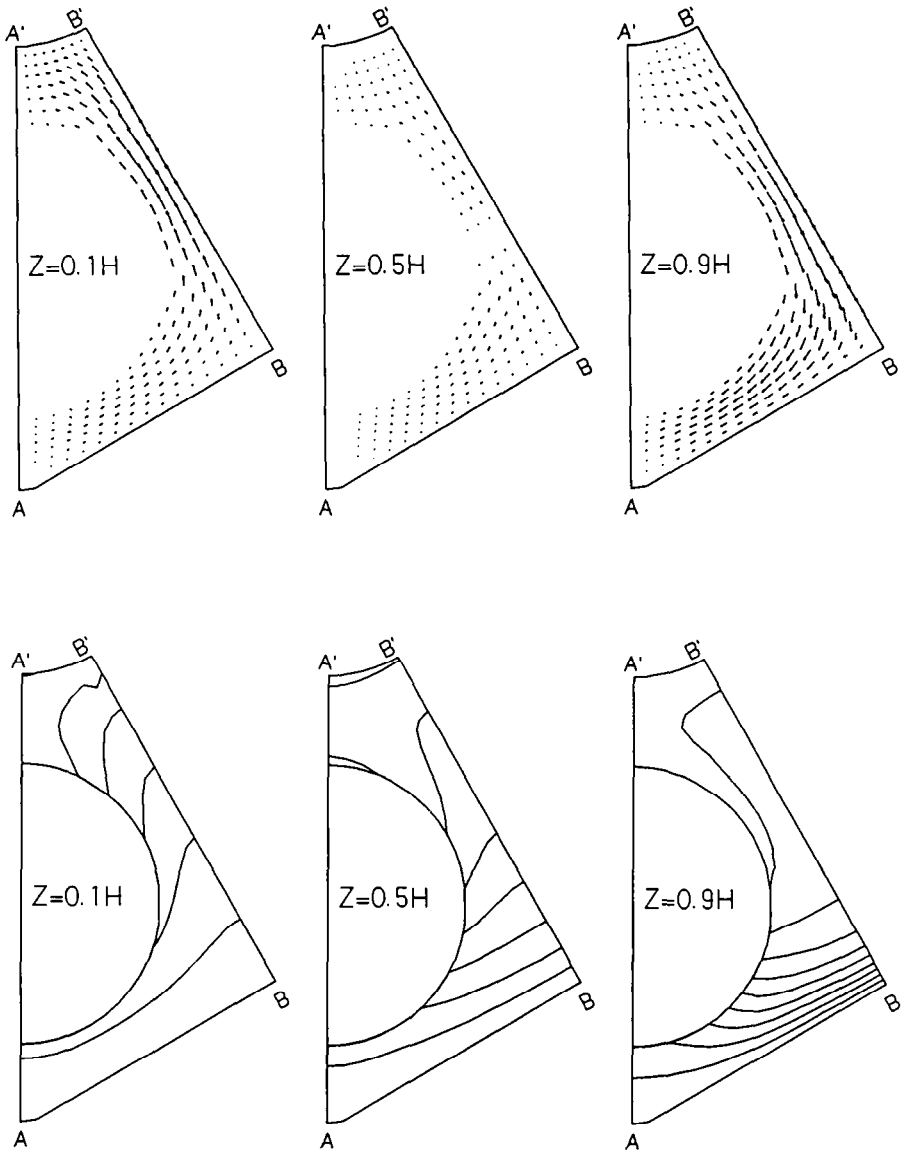

FIG. 6. (a) Velocities at selected lower, middle and upper horizontal planes for $Ra = 10^5$: $V_{2D,max} = 85.54$. (b) Isotherms at selected lower, middle and upper horizontal planes; $Ra = 10^5$.

toward the lower part of the enclosure. Figure 8 demonstrates that even in the narrow gap between the outer hot rod and the cold wall, boundary layer flows are developing, and eight isotherms, 0.1–0.8, appear in this region compared to only one isotherm (of a value of 0.1) observed for $Ra = 10^5$ shown in Fig. 5. Unlike the case of $Ra = 10^5$, since the temperature is significantly increased on the portion of the outer rod boundary that faces the cold enclosure wall, there is a weak upward flow developed along the surface, indicative of a circulating flow in this narrow channel. It is also observed that at higher Rayleigh numbers this circulating flow becomes stronger and even causes 'temperature inversion' in this area. Six isotherms (0.4–0.9) appear in the 'hot region' between the two hot rods, suggesting further cooling down of the region by the stronger flush of cold fluid from the cold wall. Figure 9 shows velocity fields and isotherms at three axial levels. The isotherms in the vicinities of the central and outer rod surfaces take shapes that are close to concentric circles, suggesting boundary temperature profiles that mainly change along the vertical direction. Almost no isotherm appears in the 'core region' away from the solid boundaries.

Boundary temperatures and heat transfer coefficients

Although the flow fields for the mixed boundary conditions look qualitatively similar to those for the isothermal boundary conditions, there are distinct differences in the heat transfer characteristics for the two cases. In the case of isothermal boundary conditions, the practical and engineering interest is on

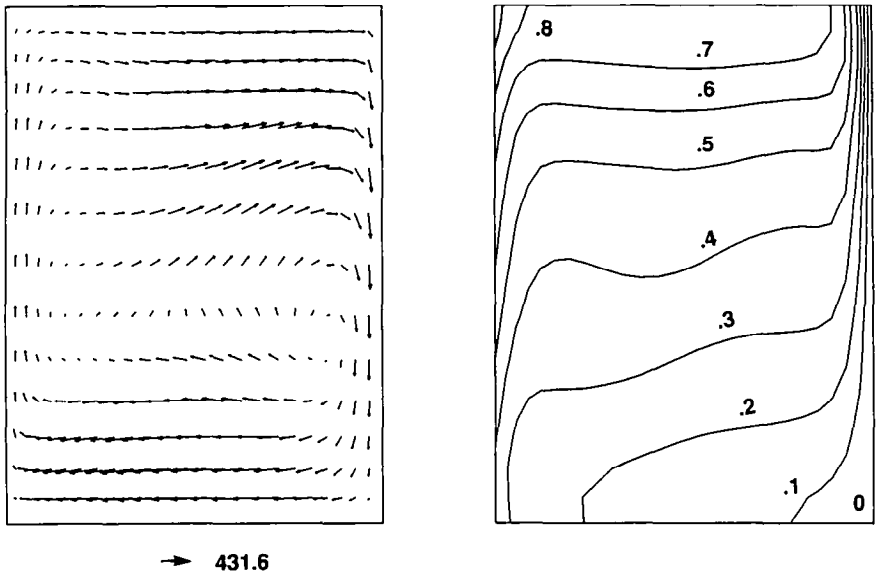

FIG. 7. Velocities and isotherms at the vertical symmetry plane B'-B for $Ra = 10^7$: $V_{2D,max} = 431.6$.

the heat fluxes across the rod and enclosure surfaces. These heat fluxes can be estimated from isotherm plots since the local heat flux vector is normal to the isotherms, and inversely proportional to the spacing between the isotherms. This is also applicable to the isothermal enclosure boundary in the case of mixed boundary conditions. As can be observed in Figs. 3, 6(b) and 9(b), increasing the Rayleigh number shifts the maximum heat flux on the cold wall toward the top end—usually at point B ($z = 0.9H$) where the hot fluid coming from the 'hot region' impinges on the cold wall (Fig. 9(a), $z = 0.9H$). This situation is similar to that observed in the case of isothermal boundary conditions. For the rod surfaces in the case of mixed boundary conditions, however, instead of the heat fluxes which are always constant by definition, the surface temperatures are the ones that are of most interest. The Nusselt number is defined in a conventional form as

$$Nu = \frac{q'_0 L'}{(T' - T'_c)k'}. \tag{8}$$

It is simply the inverse of the dimensionless tempera-

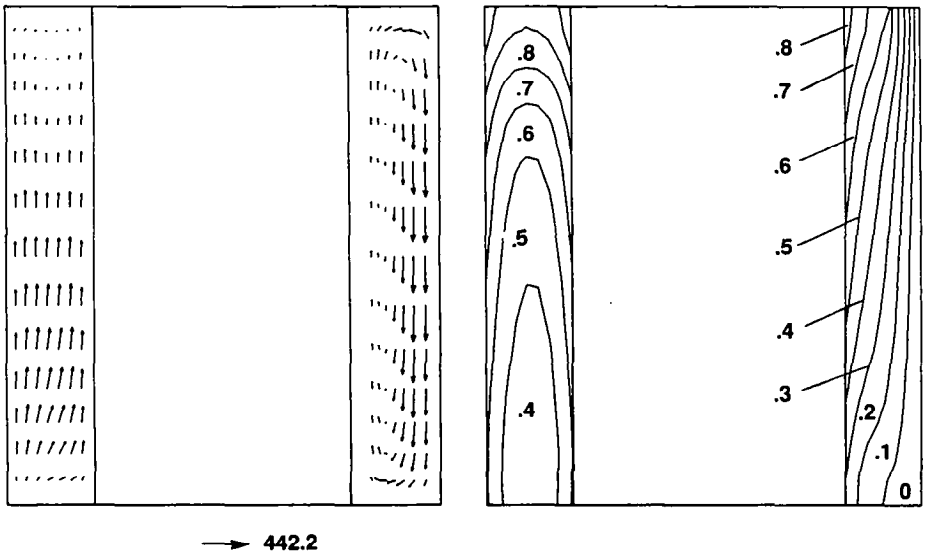

FIG. 8. Velocities and isotherms at the vertical symmetry plane A'-A for $Ra = 10^7$: $V_{2D,max} = 444.2$.

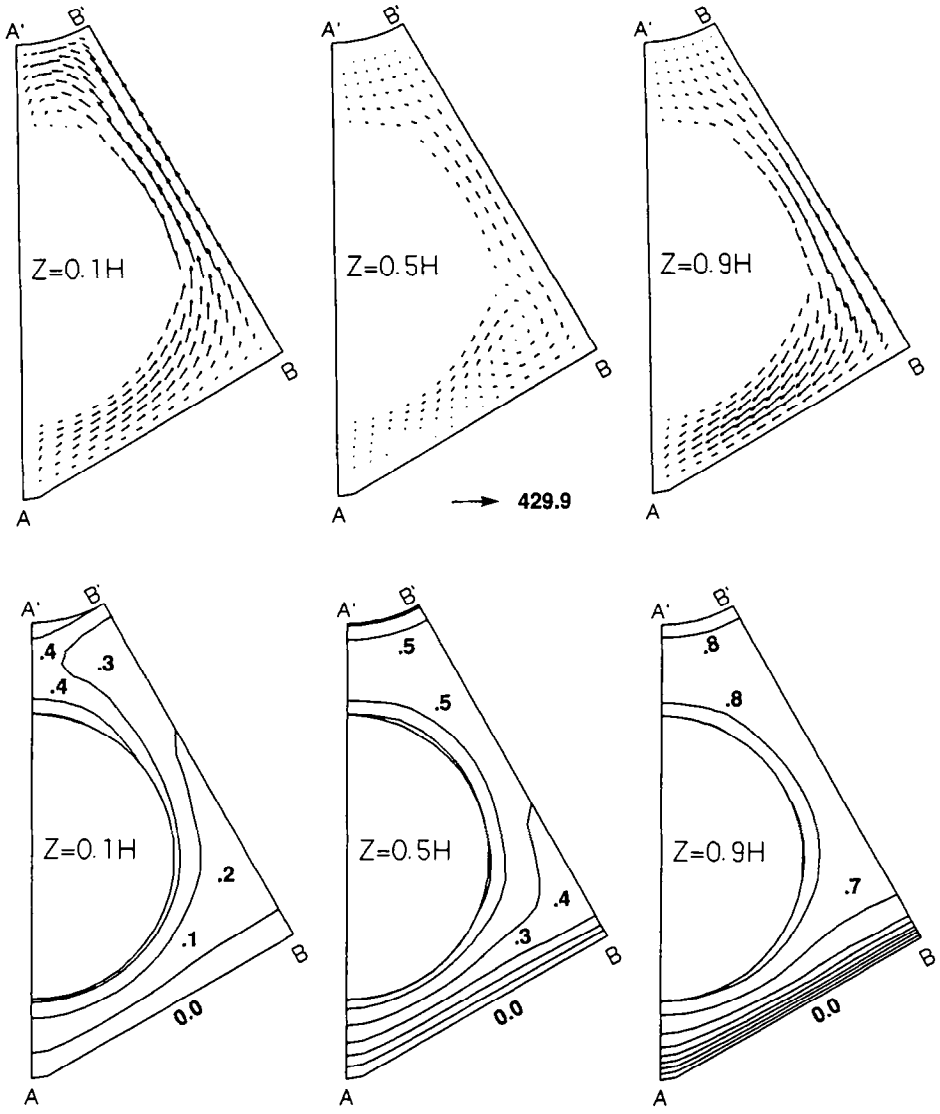

FIG. 9. (a) Velocities at selected lower, middle and upper horizontal planes for $Ra = 10^7$: $V_{2D,max} = 429.9$. (b) Isotherms at selected lower, middle and upper horizontal planes; $Ra = 10^7$.

ture. The variations of local or average Nusselt numbers, therefore, can be easily deduced from local or average boundary temperatures. The average boundary temperature on the central rod $\bar{T}_{R1}$ is obtained by integrating the local boundary temperature $T_{R1}(\xi, \zeta)$ over the rod boundary as follows:

$$\bar{T}_{R1} = \frac{1}{A}\int_{\xi}\int_{\zeta} T_{R1}(\xi,\zeta)\frac{\sqrt{\gamma}}{a}\,d\xi\,d\zeta. \tag{9}$$

The boundary temperature $T_{R1}(\xi, \zeta)$ in equation (9) is obtained by applying Fourier's law in transformed coordinates on the rod boundary as

$$-\frac{k}{J_{12}\sqrt{\gamma}}\left(\gamma\frac{\partial T}{\partial \eta} - \beta\frac{\partial T}{\partial \xi}\right) = q_0 \tag{10}$$

and A is the area of the central rod which can be calculated either from the physical dimensions or, in more general case, from the following integration over the rod surface:

$$A = \int_{\xi}\int_{\zeta}\frac{\sqrt{\gamma}}{a}\,d\xi\,d\zeta. \tag{11}$$

The local and average boundary temperature for the outer rod, T_{R2} and $\bar{T}_{R2}$, are determined in a similar way.

Figure 10 presents boundary temperature profiles at mid-height ($z = 0.5H$) along the outer rod surface, C-E-E'-C' as shown in Fig. 2, for various Rayleigh numbers that range from the pseudo-conduction to

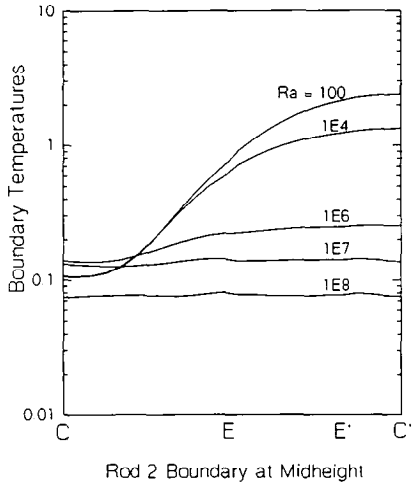

FIG. 10. Temperature profiles at $z = 0.5H$ on the outer rod boundary (along CEE'C' as shown in Fig. 2).

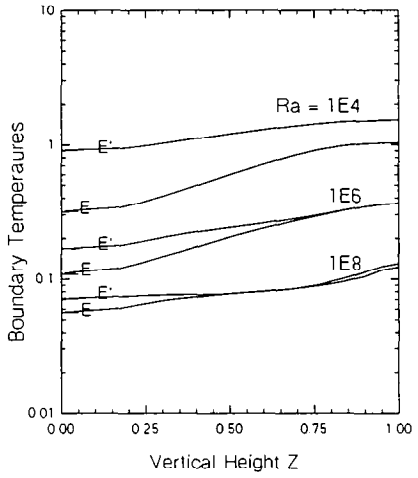

FIG. 11. Temperature profiles along two vertical lines on the outer rod boundary (E and E' as shown in Fig. 2).

boundary-layer regions. Their variations with the Rayleigh number are typical in revealing the effect of convective flow on the rod boundary temperatures. The curve for $Ra = 10^2$ corresponds to the pseudo-conduction state shown in Fig. 3; the temperature distribution at this Rayleigh number therefore represents for practical purposes all results for $Ra < 10^2$. The temperature for $Ra = 10^4$ is lower than that for the pseudo-conduction result on the portion C'-E' which faces the hot central rod, but remains unchanged on the portion C-E which faces the cold wall. This indicates that surfaces away from the cold wall may cool down faster than surfaces close to it. This interesting phenomenon occurs because the relatively strong upward flow developed in the 'hot region' between the two hot rods (Fig. 5) siphons the cold fluid down from the cold wall into this region (Fig. 6(a), $z = 0.1H$), which results in the cooling down effect. This 'siphon effect' is distinct at moderate Rayleigh numbers; only at very high Rayleigh numbers does the upward flow develop along portions of the rod surface away from the 'hot region', as previously discussed. Increasing the Rayleigh number generally reduces the variation in boundary temperature until $Ra = 10^7$ is reached at which boundary layer flows and thermal stratification are well established. Further increase in the Rayleigh number only lowers the value of the nearly uniform temperature distribution, indicating an established profile that varies only in the vertical direction.

Figure 11 is aimed at providing additional confirmation of the stratification profile. The figure shows boundary temperature profiles along two vertical lines on the outer rod surface E and E', respectively, shown in Fig. 2 as points. As the Rayleigh number is increased, the boundary temperature profiles along the two vertical lines approach each other; for $Ra = 10^8$, there exists an appreciable difference in the lower quarter section of the enclosure. This difference, however, is significantly reduced when compared with those obtained for $Ra = 10^4$ and $Ra = 10^6$.

Figure 12 shows the average boundary temperatures for the central and outer rods, $\bar{T}_{R1}$, and $\bar{T}_{R2}$ respectively. They remain almost unchanged until the Rayleigh number is increased above approximately 10^3. It is therefore reasonable to define the pseudo-conduction regime to include Rayleigh numbers less than 10^3. For higher Rayleigh numbers, both $\bar{T}_{R1}$ and $\bar{T}_{R2}$ decrease with increasing Rayleigh number. It is interesting to find that the curves for $\bar{T}_{R1}$ and $\bar{T}_{R2}$ approach the straight line of $-1/4$ slope, drawn in the figure as a reference, and at high Rayleigh numbers corresponding to boundary layer flows, the curves almost overlap with each other. This suggests that in the boundary layer region the Nusselt and Rayleigh numbers can be well correlated with $Nu = cRa^{1/4}$, an expression derived theoretically by Gill [14] and later improved upon by Bejan [15] for boundary-layer

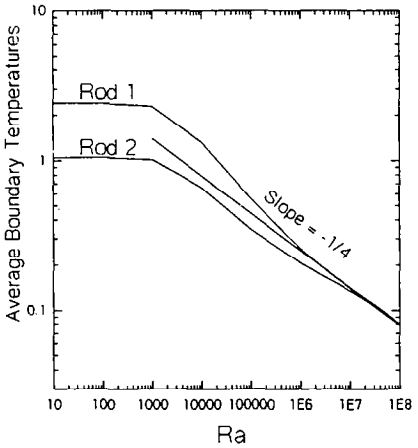

FIG. 12. Average temperatures on the central rod (Rod 1) and the outer rod (Rod 2) surfaces.

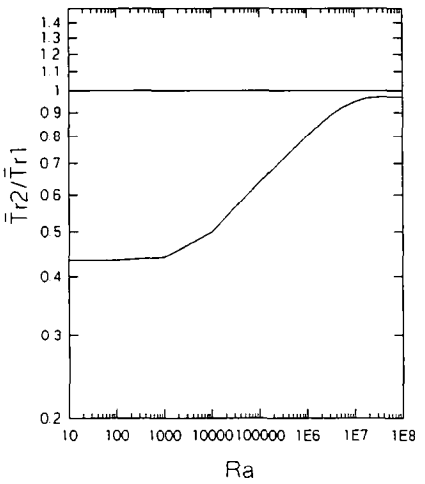

FIG. 13. The ratio of the average temperatures at the outer rod to that at the central rod surfaces.

enclosure flow with thermal stratification in a vertical rectangular cavity. Figure 13 provides additional evidence that as the Rayleigh number increases the ratio of $\bar{T}_{R2}$ to $\bar{T}_{R1}$ asymptotically as well as monotonically approaches unity, with the value at $Ra = 10^8$ being 0.97. This phenomenon can be explained with the thermal stratification at high Rayleigh numbers at which boundary layer flows are dominant. Under this condition, the interaction of a rod surface with surrounding fluid is equivalent to a situation in which the surface is placed into a thermally stratified pool; the position of the surface is, therefore, not important. It should be noted that relative positions between the rods and the other geometric factors do affect the axial temperature profile of the stratification and consequently the axial profile of boundary temperatures on the rod surfaces. A similar axial profile with little variation horizontally on the vertical rod surfaces, however, will be obtained as long as the state of stratification is reached. A similar phenomenon has been observed in the case of isothermal boundary conditions in which different rods tend to assume the same heat flux profile in the boundary-layer regime. Since Keyhani *et al.* [5] have reported experimental results showing the same tendency for a rod bundle of different rod arrangement and enclosure shape, it would be reasonable to expect that this phenomenon is independent of both the boundary conditions and the geometric factors such as the enclosure shape. This independence is fundamentally the same as that reported on boundary-layer enclosure flows in the problem of natural convection induced by heat generation in vertical porous enclosures [16].

By choosing $\bar{T}_{R2}/\bar{T}_{R1} \geqslant 0.9$ as the criterion to determine the Rayleigh number regions, we have $Ra \geqslant 10^6$ for the boundary-layer region. The region between the pseudo-conduction and the boundary-layer regions, i.e. $10^3 < Ra < 5 \times 10^6$, is therefore defined as the transitional convection region.

CONCLUSIONS

Numerical analyses have been performed in boundary-fitted coordinates for the problem of three-dimensional buoyant enclosure flow in a hot seven-pin rod bundle subject to uniform heat flux and surrounded by an isothermal, cold hexagonal enclosure, for Rayleigh numbers up to 10^8 and a Prandtl number of 0.7. Flow patterns, boundary temperature profiles or heat transfer coefficients have been obtained and presented. Comparisons have also been made of the present results for the mixed boundary conditions with those for the isothermal boundary conditions to examine the effects of boundary conditions.

Although the flow fields, isotherm distributions and heat transfer characteristics exhibit significant differences from the case of isothermal boundary conditions, the flow patterns in this geometry can be classified, in a similar way as in the case of isothermal boundary conditions, into three Rayleigh number regions. These include (a) a pseudo-conduction region in which heat is carried away almost solely by pure conduction; (b) a boundary-layer region in which thermal stratification causes boundary temperature profiles on the hot rods to vary only along the vertical direction; and (c) a transitional convection region between the above-mentioned two, in which convective flow is strong enough to result in apparent deviation of rod boundary temperatures from the pseudo-conduction state and the 'siphon effect', but not to cause thermal stratification. The corresponding Rayleigh number ranges for these regions are: $Ra \leqslant 10^3$ for the pseudo-conduction region, $10^3 < Ra < 5 \times 10^6$ for the transitional convection region and $Ra \geqslant 5 \times 10^6$ for the boundary-layer region.

The flow is generally driven by a downward flow along the cold enclosure wall and an upward flow in the 'hot region' between the central and outer rods. Siphoned by this strong upward flow, the cold fluid down from the cold wall flows horizontally at the bottom region toward the 'hot region', by-passing the outer rod surface, and turns its direction to flow upward when it reaches the 'hot region'. Only when the Rayleigh number is high enough to cause boundary layer flow, does an upward flow develop along the portions of the outer-rod boundary that are away from the 'hot region'. This 'siphon effect' observed at moderate Rayleigh numbers is the cause of an interesting phenomenon that shows that surfaces away from the cold wall cool down faster than surfaces close to it.

In the boundary-layer regime, as a result of thermal stratification that occupies an increasingly large 'core region' as the Rayleigh number increases, the rods at different positions tend to achieve nearly the same average boundary temperature or consequently the same overall heat transfer coefficient. This agrees with experimental observations for a rod bundle of different configuration [5]. It is concluded that in this

regime, the Nusselt and Rayleigh numbers can be well correlated with $Nu = cRa^{1/4}$, which is in the same form as was theoretically derived for boundary-layer enclosure flows in a vertical rectangular cavity.

Acknowledgement—The support of the Oak Ridge Associated Universities through Contract #3C-56703 and Grant 300281/I91-15 from Howard University are gratefully acknowledged.

REFERENCES

1. K. T. Yang, Natural convection in enclosures, *Handbook of Single-Phase Convective Heat Transfer* (Eds. S. Kakac, R. K. Shah and W. Aung). Wiley, New York (1987).
2. G. D. Mallinson and G. de Vahl Davis, Three-dimensional natural convection in a box, *J. Fluid Mech.* **83,** 1–13 (1977).
3. H. Ozoe, K. Yamamoto, H. Sayama and S. W. Chuchill, Natural convection patterns in a long inclined rectangular box heated from below, *Int. J. Heat Mass Transfer* **20,** 131–139 (1977).
4. Y. Takata, K. Iwashige, K. Fukuda and S. Hasegawa, Three-dimensional natural convection in an inclined cylindrical annulus, *Int. J. Heat Mass Transfer* **27,** 747–754 (1984).
5. M. Keyhani, F. A. Kulacki and R. N. Christensen, Experimental investigation of free convection in a vertical rod bundle—a general correlation for Nusselt numbers, *J. Heat Transfer* **107,** 611–623 (1985).
6. B. C. J. Chen, W. T. Sha, M. L. Doria, R. C. Schmitt and J. F. Thompson, BODYFIT-1FE: a computer code for three-dimensional steady-state/transient single-phase rod-bundle thermal hydraulic analysis, NUREG/CR-1874, ANL-80-127, November 1980.
7. A. S. Chorin, The numerical solutions of the Navier–Stokes equations for an incompressible fluid, *Bull. Am. Math. Soc.* **73,** 928–931 (1967).
8. E. K. Glakpe, C. B. Watkins, Jr. and B. Kurien, Solution of three-dimensional natural convection about a vertical square rod in a cylindrical enclosure, *Int. J. for Numerical Methods in Fluids* **7,** 155–173 (1987).
9. S. V. Patankar, *Numerical Heat Transfer and Fluid Flow.* Hemisphere (1980).
10. Y. F. Rao and E. K. Glakpe, Three-dimensional natural convection in a rod bundle—A numerical study in boundary-fitted coordinates, *Numerical Methods in Thermal Problems,* Vol. VII, Part I, 446–456 (1991).
11. J. F. Thompson, *Numerical Grid Generation.* Elsevier (1982).
12. P. J. Roache, *Computational Fluid Dynamics.* Hermosa (1982).
13. B. Kurien, Three-dimensional computations of natural convection inside a vertical enclosure, M.S. Thesis, Howard University, Washington, D.C. (1984).
14. A. E. Gill, The boundary layer regime for convection in a rectangular cavity, *J. Fluid Mech.* **26,** 515–536 (1966).
15. A. Bejan, Note on Gill's solution for free convection in a rectangular enclosure, *J. Fluid Mech.* **90,** 561–563 (1966).
16. Y. F. Rao and B. X. Wang, Natural convection in vertical porous enclosures with internal heat generation, *Int. J. Heat Mass Transfer* **34,** 247–252 (1991).